Available online at www.sciencedirect.com
SCIENCE DIRECT®
C. R. Physique 4 (2003) 621–637
COMPTES RENDUS PHYSIQUE

Semiconductor lasers/Lasers semiconducteurs

GaSb-based mid-infrared 2–5 µm laser diodes

André Joullié [a,*], Philippe Christol [b]

[a] *Centre d'électronique et de microoptoélectronique de Montpellier (CEM2), UMR CNRS n°5507, Université de Montpellier II, sciences et techniques du Languedoc, case 067, 34095 Montpellier cedex 05, France*
[b] *Laboratoire de physique des matériaux (LPM), faculté des sciences d'Avignon, Université d'Avignon et Pays de Vaucluse, 33, rue Pasteur, 84000 Avignon, France*

Received 3 January 2003; accepted 15 March 2003

Presented by Guy Laval

Abstract

Laser diodes emitting at room temperature in continuous wave regime (CW) in the mid-infrared (2–5 µm spectral domain) are needed for applications such as high sensitivity gas analysis by tunable diode laser absorption spectroscopy (TDLAS) and environmental monitoring. Such semiconductor devices do not exist today, with the exception of type-I GaInAsSb/AlGaAsSb quantum well laser diodes which show excellent room temperature performance, but only in the 2.0–2.6 µm wavelength range. Beyond 2.6 µm, type-II GaInAsSb/GaSb QW lasers, type-III 'W' InAs/GaInSb lasers, and interband quantum cascade lasers employing the InAs/Ga(In)Sb/AlSb system, all based on GaSb substrate, are competitive technologies to reach the goal of room temperature CW operation. These different technologies are discussed in this paper. ***To cite this article: A. Joullié, P. Christol, C. R. Physique 4 (2003).***

Résumé

Diodes laser à base GaSb pour moyen infrarouge (2–5 µm). Les diodes laser émettant en continu à température ambiante dans le moyen infrarouge (domaine spectral 2–5 µm) sont réclamées pour des applications telles que la spectroscopie d'absorption par diodes lasers accordables (TDLAS) et le contrôle de l'environnement. Aujourd'hui de tels composants semiconducteurs n'existent pas, à l'exception de diodes laser à puits quantiques de type-I GaInAsSb/AlGaAsSb qui présentent d'excellentes performances à température ambiante, mais uniquement dans le domaine 2.0–2.6 µm. Au delà de 2.6 µm, les lasers à puits quantiques de type-II à GaInAsSb/GaSb, les lasers « W » utilisant le système de type-III InAs/GaInSb, et les lasers à cascade quantique à transitions inter-bandes dans le système InAs/Ga(In)Sb/AlSb, tous élaborés sur substrat GaSb, constituent des filières compétitives pour atteindre l'objectif d'un fonctionnement en continu à température ambiante. Ces différentes technologies sont discutées dans cet article. ***Pour citer cet article : A. Joullié, P. Christol, C. R. Physique 4 (2003).***

Keywords: Laser diodes; Mid infrared; GaSb; Type-I lasers; Type-II lasers; 'W' lasers; Quantum cascade lasers

Mots-clés : Diodes lasers ; Moyen infrarouge ; GaSb-Lasers de type-I ; Lasers de type-II ; Lasers « W » ; Lasers à cascade quantique

* Corresponding author.
E-mail address: joullie@univ-montp2.fr (A. Joullié).

1631-0705/$ – see front matter
doi:10.1016/S1631-0705(03)00098-7

1. Introduction

Light emitters operating in the mid-infrared (MIR) wavelength domain (2–5 μm) are desirable for many applications in telecommunications and molecular spectroscopy. Optical telecommunications can be achieved through the 2–2.5 μm and 3.5–4 μm high transparency atmospheric windows [1]. Gas detection with a high resolution can be developed because a lot of polluting gases and combustion products have strong absorption lines in the mid-IR region: NH_3 (2.1 μm), HF (2.5 μm), CH_4 (2.35 μm and 3.3 μm), HCHO (3.5 μm), HCl (3.5 μm), N_2O (3.9 μm and 4.5 μm), SO_2 (4 μm), CO_2 (4.25 μm) and CO (2.3 μm and 4.6 μm) [2].

The use of MIR semiconductor lasers emitting at room temperature offers rich possibilities for areas such as atmospheric pollution monitoring, industrial process control, leak detection, automotive engine exhaust analysis, drug detection, aid for the medical diagnosis of disease. Other important applications include laser surgery, rangefinding, and IR countermeasures. These applications require light emitters having a small spectral width and high optical power and brightness. Semiconductor laser diodes can fulfil these criteria. The goal is to obtain devices operating in continuous mode (CW) at room temperature, promising compact sources more widely applicable than conventional technology such as optical parametric oscillators. For gas analysis, tunable diode laser absorption spectroscopy (TDLAS) is classically employed [3]. CW output power of 1–10 mW and single optical mode emission are required, with the ability to tune the lasing wavelength in a wide spectral domain. For other applications much higher CW output powers (∼1 W) are needed.

Infrared laser emission was first demonstrated at 3.1 μm from InAs [4], at 5.3 μm from InSb [5,6] and at much longer wavelengths from PbTe and PbSe [7] p-n junction diodes. During the 1980s, standard mid-IR lasers were exclusively fabricated from narrow gap lead and lead-tin based IV-VI semiconductors PbTe, PbSe, PbS, PbSnTe, PbSnSe and PbSSe. Typical devices were diffused laser diodes, operating at low temperature (4–77 K) in the wavelength range 4–30 μm, the shortest wavelength being limited by the energy gap of PbS or PbTe, to approximately either 4 μm or 5.5 μm at 77 K [7]. A noticeable improvement in IV-VI laser properties was achieved with double heterostructure (DH) lasers, and then with multi-quantum well (MQW) lasers, fabricated using the advanced growth techniques such as liquid phase epitaxy (LPE), hot wall epitaxy (HWE) and molecular beam epitaxy (MBE) techniques. The laser structures, grown on PbS, PbSe or PbTe substrates, could operate beyond 100 K CW in the wavelength range 3 to 30 μm, using as active layers PbEuSSe or PbSrSe for the short wavelength region 3–4 μm [8–11], PbEuSeTe or PbEuSe for the 4–8 μm range, and PbSnTe or PbSnSe for wavelengths beyond 8 μm [12]. Up to the end of the 1990s, the IV-VI lasers remained the only commercially available among infrared semiconductor lasers.

In the last years impressive results were obtained with III-V quantum well lasers designed by band structure engineering [13,14]. The aim of band structure engineering is to imagine new laser structures able to reach small non-radiative Auger recombination (which is one of the main loss mechanisms in long wavelength lasers) and high optical efficiency. Contrary to IV-VI systems, III-V heterostructures possess strong differences in band gap energy and band discontinuity allowing the formation of deep and confining quantum wells. Besides, the possibility of growing strained layers by MBE offers matter for imagining and fabricating complex but high-performing laser structures. In 2000, four III-V laser technologies have emerged in this way for laser emission in the mid-infrared: (i) interband lasers including in their active zone GaInAsSb/AlGaAsSb type-I or GaInAsSb/GaSb type-II quantum wells (QWs) [15–22]; (ii) type-III 'W' lasers based on the InAs/GaInSb system [23–26]; (iii) quantum cascade lasers (QCLs) which employ conduction intersubband radiative transitions in the GaInAs/AlInAs system [27–33]; and (iv) interband quantum cascade lasers (ICLs) which associate interband transitions and cascade effect in the type-III InAs/GaInSb system [34–36]. Excellent performance was obtained in pulsed regime at room temperature or near room temperature from these different technologies.

Nevertheless there is still no semiconductor laser diode presently able to work at room temperature in a continuous regime in the MIR wavelength region, with the exception of GaInAsSb injection lasers which could operate CW in the shortest wavelength domain up to 2.7 μm [15]. GaSb-based semiconductor laser diodes are a way of reaching the goal of CW RT operation in a wide range of MIR wavelengths. In this paper, we present the performance (expected or already realized) of different laser structures, all employing antimoniure alloys and grown on GaSb substrates: type-I GaInAsSb/AlGaAsSb QW lasers, type-II GaInAsSb/GaSb QW lasers, type-III 'W' lasers based on InAs/GaInSb and InAsSb/GaSb systems, and InAs/AlSb quantum cascade lasers.

2. Mid-infrared laser features

2.1. Basic laser structure

A schematic drawing of a GaSb-based laser diode with a Fabry–Pérot cavity is shown in Fig. 1. The active zone is sandwiched between two thick (2–3 μm) confining layers of high band gap and low refractive index Al-rich AlGaAsSb solid solution lattice-matched to the substrate (cladding layers). Classically, the substrate and the first cladding layer are n-type (tellurium doped), the

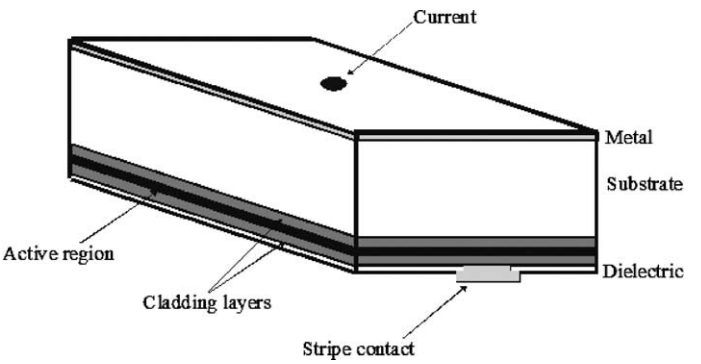

Fig. 1. Schematic diagram of a laser diode.

active region is undoped, and the second confining layer has a p-type conductivity (beryllium doped). A thin and highly doped GaSb layer is grown at the top of the structure for contacting. It is often recommended to insert a layer of graded composition between the substrate and the adjacent confining layer, or generally between each confining layer and the adjacent low band gap material, in order to facilitate carrier injection and reduce the series resistance of the laser diode. InAs/AlSb superlattice has been proposed as material for cladding layers [37]. Compared to AlGaAsSb quaternary alloy, the superlattice provides a straightforward lattice-match to the substrate and circumvents the need for a tellurium dopant.

In QW lasers the active region consists of quantum wells shared in the centre of a spacer layer (called waveguide layer) which has a lower band gap energy and higher refractive index than those of the two adjacent cladding layers. The role of this spacer layer is to reduce the penetration of light in the cladding layers in order to decrease optical absorption loss [38]. QW lasers can be classified into three categories, depending on the nature of the band alignment at the well-barrier interface (Fig. 2): nested (type-I), staggered (type-II) and broken gap (type-III). In the first case electrons and holes are confined into the same material (Fig. 2(a)), while in the two other cases carriers are spatially separated into the adjacent layers. As a consequence indirect radiative recombinations are generated (Fig. 2(b) and (c)). Note that the type-III band alignment is a particular case of the type-II alignment where the conduction band of the well is placed below the valence band of the barrier (Fig. 2(c)).

The knowledge of conduction and valence band-offsets at the heterostructure interface is fundamental for the design of the QW laser. Using band gap values, extracted from standard parameters of III-V compounds [39,40], and valence band-offset values of III-V unstrained hetero-interfaces, calculated from the data of Tsou [41], it is possible to determine the type of band alignment for a number of III-V unstrained heterostructures.

Fig. 3 presents a schematic view at scale of the band-edge alignments of some unstrained III-V binary systems. We can remark that hetero-interfaces between arsenides (or antimonides) are always type-I, whereas interfaces between arsenides and antimonides can be type-I (InSb/AlAs, GaSb/AlGaAsSb), type-II (InAs/AlSb, GaInAsSb/GaSb, InAsSb/InAs) and type-III (InAs/GaSb, InAs/GaInSb). Fig. 3 also shows that extremely deep quantum wells (of the order of 1 eV) are realized in the conduction band by associating compounds with type-II or type-III band offsets (e.g., InAs/AlSb, InAs/GaSb).

2.2. State of the art of mid-infrared laser performance

In Fig. 4 is reported the maximum temperature of operation $T_{\max}$ achieved to date from semiconductor laser diodes emitting CW in the mid-IR wavelength region. Two groups clearly appear. For $\lambda < 2.7$ μm, GaSb-based type-I GaInAsSb/AlGaAsSb and type-II GaInAsSb/GaSb QW lasers could emit CW at and above room temperature, best results being obtained with type-I lasers ($T_{\max} = 130\,^{\circ}\mathrm{C}$ at $\lambda = 2.3$ μm [21]). Beyond 2.7 μm there is no laser system operating CW in the mid-infrared at room temperature. Maximum CW operation temperatures are 195 K for type-III 'W' InAs/GaInSb lasers at $\lambda = 3.3$ μm [25], 223 K for PbEuSeTe/PbTe QW laser at $\lambda = 4.2$ μm [42], and 210 K for GaInAs/InAlAs strained QCL at $\lambda = 5.2$ μm [33]. It can be noted that, except for quantum cascade lasers, the maximum temperature of operation $T_{\max}$ regularly decreases with the wavelength.

In Fig. 5 the maximum CW output power per facet exhibited by the devices is shown. The two groups of laser diodes are again observed. High CW optical power were reported from type-I GaInAsSb/AlGaAsSb QW lasers (1.9 W at 2.0 μm [43,44], 680 mW at 2.3 μm [45], 1 W at 2.5 μm [46]). A strong decline of the performances is visible beyond 2.7 μm. For the second group of III-V systems, noticeable output power was measured at low temperature ($T = 80$ K). The highest reported CW powers per facet are 140 mW at 3.25 μm for type-III 'W' InAs/GaInSb laser [25], 215 mW at 3.4 μm for type-I InAsSb/AlInAsSb QW laser [47], 100 mW at 3.7 μm for InAs/GaInSb ICL [48] and 150 mW single mode at 4.6–4.7 μm for GaInAs/AlInAs QCL [28]. Lead salt lasers exhibit weak output powers, of the mW order [11].

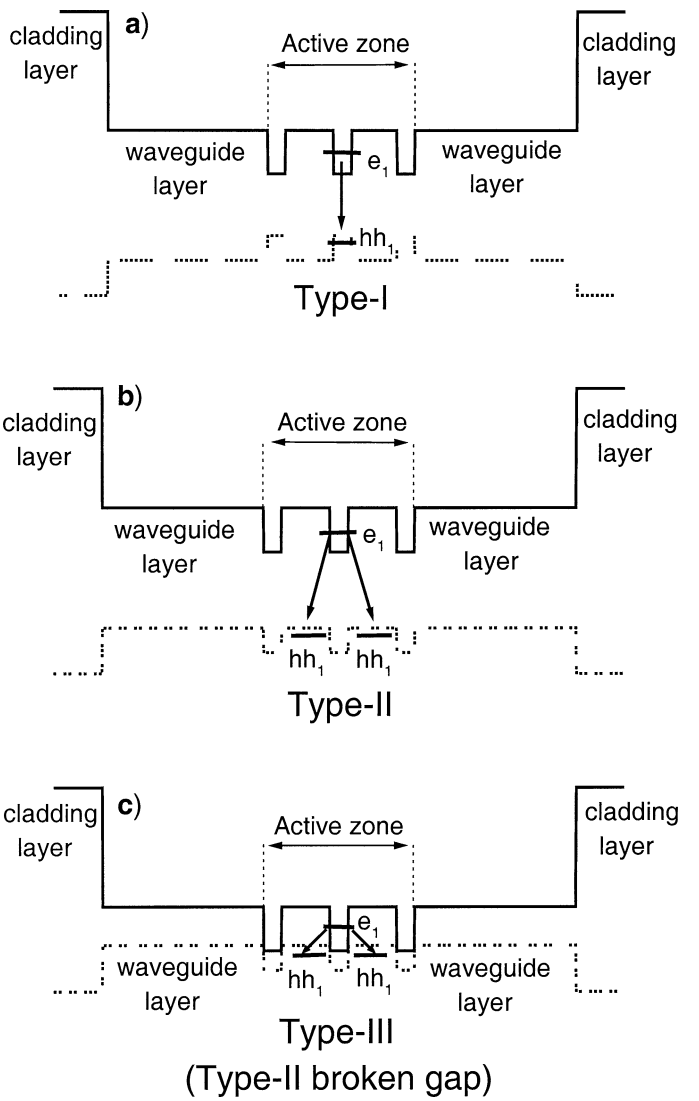

Fig. 2. The different types of band alignment: (a) type-I; (b) type-II; (c) type-III (often called type-II broken gap, and by word confusion, type-II). The fundamental electron–hole transition e1–hh1 is showed.

2.3. Limiting physical parameters

The main physical parameters responsible for the performance limitations at long wavelengths can be found by considering the threshold current density of a laser diode. The different contributions to the current in an injection laser are the non-radiative Schockley–Hall–Read (SHR) recombinations on deep levels, the interband spontaneous recombinations, and the non-radiative Auger recombinations [49]:

$$J = qd(R_{\mathrm{nr}} + R_{\mathrm{sp}} + R_{\mathrm{Auger}}). \tag{1}$$

In Eq. (1) J is the current density, d is the width of the active region, R_{nr} is the SHR recombination rate, R_{sp} the radiative recombination rate and R_{Auger} the Auger recombination rate. Eq. (1) is described by the phenomenological equation:

$$J = qd\left(AN + BN^2 + CN^3\right), \tag{2}$$

where N is the concentration of the injected carriers (supposed much higher than equilibrium carrier concentrations of the active region). A is the non-radiative SHR coefficient, B is the spontaneous emission coefficient and C is the Auger coefficient. The

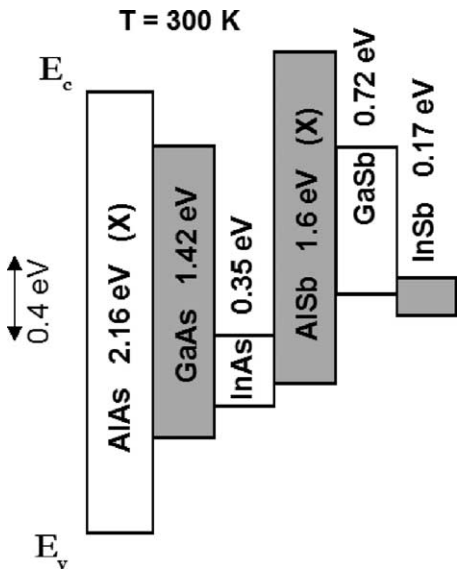

Fig. 3. Conduction and valence band edges of unstrained III-V binary compounds showing the conduction and valence band discontinuities at the hetero-interfaces for adjacent systems.

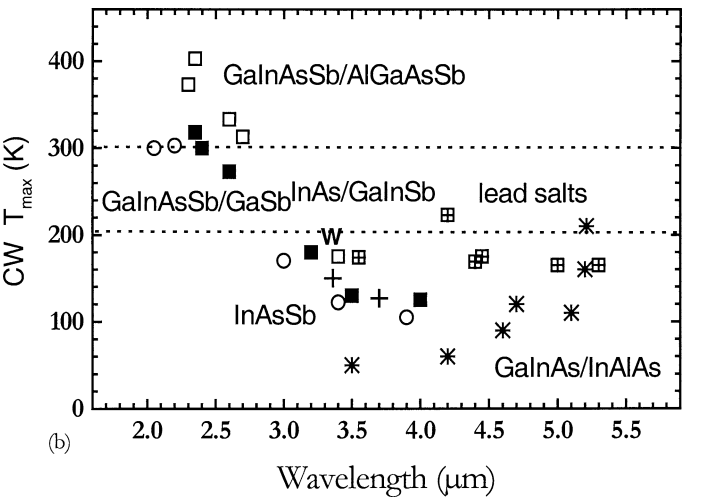

Fig. 4. Maximum operating temperature of semiconductor laser diodes operating CW in the mid-infrared. ○ Sb-based double heterostructure lasers, □ Sb-based type-I MQW lasers, ■ Sb-based type-II MQW lasers, W Sb-based 'W' lasers, + Sb-based type-II interband cascade lasers (ICLs), ∗ Inter sub-band quantum cascade lasers (QCLs), ⊞ IV-VI lead salt lasers.

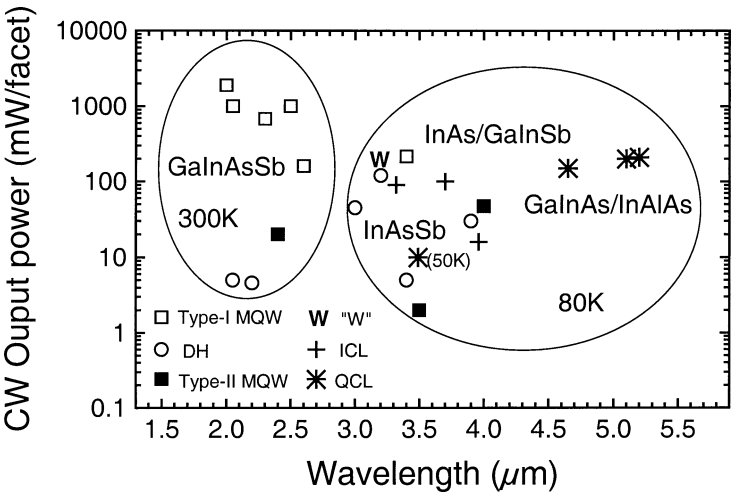

Fig. 5. Ouput power of semiconductor laser diodes operating CW in the mid-infrared. ○ Sb-based DH lasers, □ Sb-based type-I MQW lasers, ■ Sb-based type-II MQW lasers, W Sb-based 'W' lasers, + Sb-based type-II interband cascade lasers (ICLs), ∗ Inter sub-band quantum cascade lasers (QCLs).

laser threshold is obtained when the modal gain $G_{\mathrm{mod}}(N)$, which increases with the injected carrier concentration N, becomes equal to the total optical losses α_{total}:

$$G_{\mathrm{mod}}(N = N_{\mathrm{th}}) = \Gamma G_{\mathrm{max}}(N = N_{\mathrm{th}}) = \alpha_{\mathrm{total}} = \alpha_{\mathrm{int}} + \alpha_{\mathrm{FP}}. \tag{3}$$

Γ is the optical confinement factor, G_{max} is the maximum optical gain for an injected carrier concentration N, α_{int} is the internal loss coefficient and α_{FP} is the mirror loss of the Fabry–Pérot cavity. The carrier concentration at threshold N_{th} is then determined by Eq. (3), and the threshold current density J_{th} is given by:

$$J_{\mathrm{th}} = qd\left(AN_{\mathrm{th}} + BN_{\mathrm{th}}^2 + CN_{\mathrm{th}}^3\right). \tag{4}$$

For long wavelength lasers, two parameters are of critical importance: (i) the internal losses, and particularly losses due to *free carrier absorption* which strongly increase with wavelength [50,51]. This increase induces an increase of the carrier concentration at threshold N_{th}. (ii) The *Auger nonradiative coefficient* which increases exponentially with the wavelength [49, 52]. As a consequence, the Auger rate, which varies as CN^3, is dramatically increased, and the Auger contribution to the threshold current becomes the dominant mechanism at room temperature.

In the free carrier absorption mechanism, the photon disappears by collision with a free carrier, electron or hole, which increases its energy. That increase requires a change in the k wave vector with the aid of a diffusion mechanism (impurity, optical phonon). The free carrier absorption mechanism is not simple to quantify. A practical equation is:

$$\alpha_{\text{fc}} = K \cdot \left[N\ (\text{cm}^{-3})/10^{17}\right] \cdot \left[\lambda\ (\mu\text{m})/9\right]^{p}, \tag{5}$$

where K and p are constants dependent on a given material [51,53]. Fig. 6 shows the variation of the free carrier absorption coefficient α_{fc} of different mid-IR materials as a function of the carrier concentration N, for a wavelength $\lambda = 3.5$ μm. One can see that the α_{fc} value for AlAsSb material, which is currently used as the cladding layer in a mid-IR laser structure, becomes high ($\sim$20 cm^{-1}) at carrier concentrations around 10^{18} cm^{-3} which are typical values for injected carriers at threshold. Inversely, the free carrier absorption coefficient of GaSb, InAs and $Al_{0.35}Ga_{0.65}As_{0.03}Sb_{0.97}$ materials, which are usually employed as waveguide layers, remains reasonably small ($\sim$1–3 cm^{-1} at $N = 10^{18}$ cm^{-3}).

Two examples of Auger recombination processes are given in Fig. 7. They concern the CHCC and CHHH mechanisms in type-III quantum wells. In the CHCC process the conduction to heavy hole CH recombination 1–2 is accompanied by an electron transition 3–4 to a higher energy conduction band state CC. In the CHHH process the CH recombination is accompanied by a hole transition 3–4 to a higher energy valence band state HH. In that mechanism if H1H3 transition energy is equal to the E1H1 transition energy, the Auger CHHH mechanism is highly probable. However, the band structure can be designed to suppress this 'resonance'. In this case, the multi-hole CHHH process becomes energetically unfavorable, and cannot occur.

Such considerations brought a number of authors to predict extremely small Auger coefficients for type-III quantum wells [54–56]. In fact the reduction of Auger effect in this kind of heterostructures is real, but much less than theoretically estimated, as shown in Fig. 8. In Fig. 8 the Auger coefficients for a number of mid-IR materials experimentally determined at room temperature or near room temperature by Meyer et al. [57], Vurgaftman et al. [26], Joullié [20], and Pautrat [58] are reported. The following findings can be drawn from these experiments. In the 2–5 Fig. 8 μm mid-IR wavelength domain, the Auger coefficient of III-V compounds strongly increases with temperature (from $\sim 10^{-28}$ cm^6/s to $\sim 10^{-26}$ cm^6/s). In the wavelength range 2.0–2.6 μm type-II staggered GaInAsSb/GaSb quantum wells show Auger coefficients smaller than those of type-I GaInAsSb/AlGaAsSb quantum wells. In the 3–5 μm wavelength region, InAs/GaInSb type-III 'W' quantum wells show smaller Auger coefficients than bulk material (InAs, InAsSb). This reduction is noticeable (its corresponds to a factor $\sim$5), but it is far from that predicted by calculations. Around 4 μm, the Auger coefficient of lead salts is strongly inferior to that of

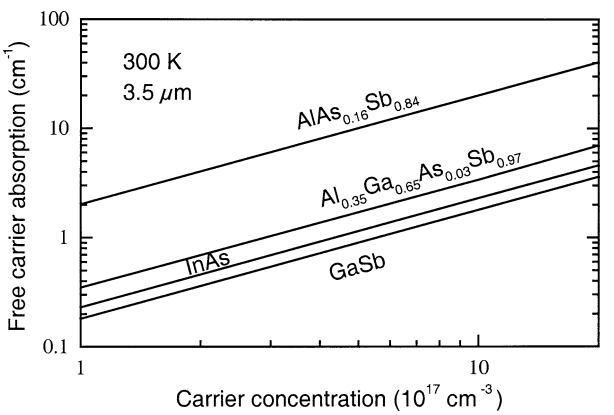

Fig. 6. Free carrier absorption coefficient versus free electron concentration of different mid-infrared materials calculated for a wavelength of 3.5 μm.

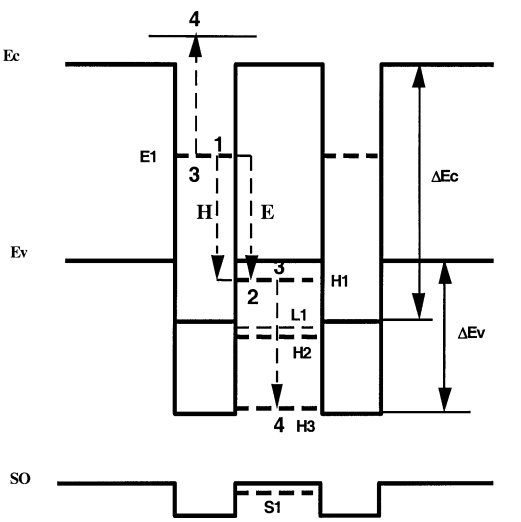

Fig. 7. Schematic band diagram of a type-III quantum wells indicating CHCC and CHHH Auger process. H and E give the two possible recombination channels of electron 1 and hole 2. The numbers 1 and 3 denote initial states of the particles, 2 and 4 denote the final states.

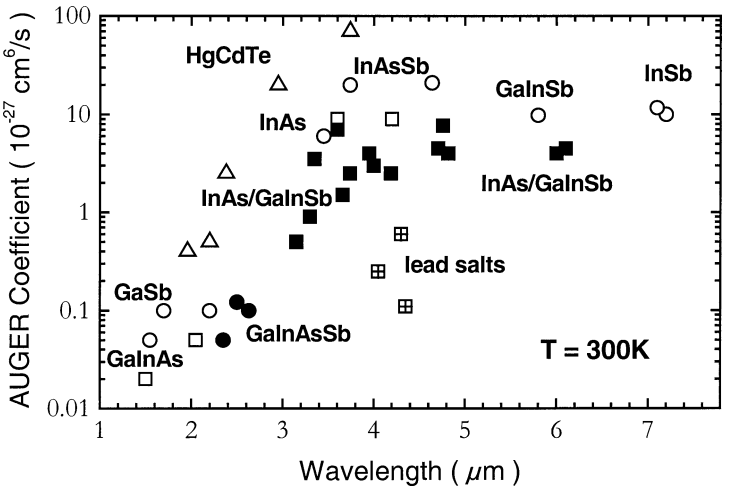

Fig. 8. Measured Auger coefficients versus gap wavelength of mid-IR semiconductor materials. ○ bulk materials, □ type-I GaInAsSb/AlGaAsSb and InAsSb/AlInAsSb MQWs, ● type-II GaInAsSb/GaSb MQWs, ■ type-III InAs/GaInSb MQWs, ⊞ IV-VI lead salts.

III-V systems by a factor superior to 10. This explains the high temperature operation of lead salt devices (Fig. 4), while small radiative efficiency can explain their weak optical power.

3. Type-I GaInAsSb/AlGaAsSb laser diodes

Laser diodes based on the GaInAsSb/AlGaAsSb system have the structure of Fig. 1 with an active region employing compressively strained (1–2%) quantum wells of $Ga_{1-x}In_xAs_ySb_{1-y}$, and GaSb lattice-matched barriers of $Al_xGa_{1-x}As_ySb_{1-y}$ having a moderate aluminium content ($x = 0.20$–0.35). They are classically grown by MBE. The type-I GaInAsSb/AlGaAsSb system offers the following advantages:

- a strong electrical confinement for electrons ($\Delta Ec \sim 300$–400 meV) for the increase of radiative efficiency;
- an important difference in the refractive index ($\Delta n \sim 0.4$) of AlGaAsSb spacer and $Al_{0.9}Ga_{0.1}As_{0.08}Sb_{0.92}$ cladding layers, for high optical confinement;
- a small Auger coefficient ($C_{\text{Auger}} \sim 5 \times 10^{-29}$ cm^6/s at $\lambda = 2.05$ μm [20]) for the reduction of threshold current. This small value is the result of two factors: the vanishing of the 'resonance' between the effective band gap E1H1 and the spin split-off energy transition H1S1, resonance which occurs for GaSb and gallium-rich alloys [59], and the low in-plane mass for holes due to strain with as a consequence an increase of the Auger activation energy [60].

The conduction and valence band energy levels of a typical laser structure, designed for 2.3 μm wavelength emission, are schematically depicted in Fig. 9. The thickness of the spacer must be sufficient to avoid excessive penetration of the emitted light into the cladding layers. If this is not the case, there is strong absorption of photons by free carriers in the doped cladding layers, inducing high internal optical losses (cf. Fig. 6).

Ridge lasers with cleaved Fabry–Pérot (FP) cavity of 1–2 mm length are the standard laser devices. They use broad stripe contact (100 μm) for high power emission and narrow stripe contact (5–10 μm) for single mode transverse operation. A cross section of a ridge laser is shown in Fig. 10. The ridge geometry is generally obtained by reactive ion etching in a $SiCl_4$/Ar plasma, etching being stopped in the p-AlGaAsSb cladding layer just above the active region. A too deep etching favors lateral waveguide modes; a too shallow etching increases the laser threshold because of the lateral current spreading. The wafer is planarized by a thick layer of polymer so that the device can be indium-soldered p-side down onto cooled copper heatsink. That situation promotes the heat evacuation from the device through the support. In order to collect the maximum output power, the FP facets are often coated with antireflection layer (3–5%) at the front facet, and high reflection layer (95–97%) at the rear facet. The reflectivity of uncoated facets is around 30%. The obtention of low resistivity ohmic contacts is of primary importance in CW operation. Using a Au (or Au/Te) sputtered layer for n-type GaSb and sputtered Au/Zn for p-type GaSb, specific contact resistivities inferior to 10^{-5} Ωcm^2 are obtained. The series resistance is ∼0.1 Ω for broad stripe lasers and ∼1 Ω for narrow ridge lasers.

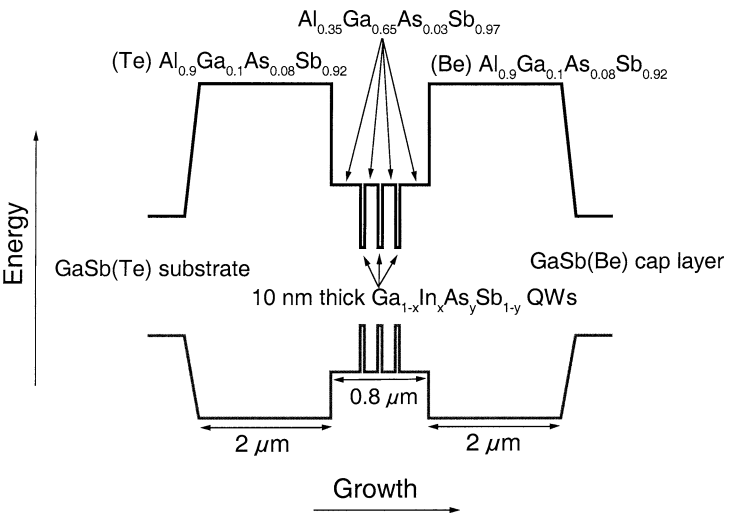

Fig. 9. Schematic energy band diagram of a type-I GaInAsSb/AlGaAsSb diode laser emitting at 2.3 µm.

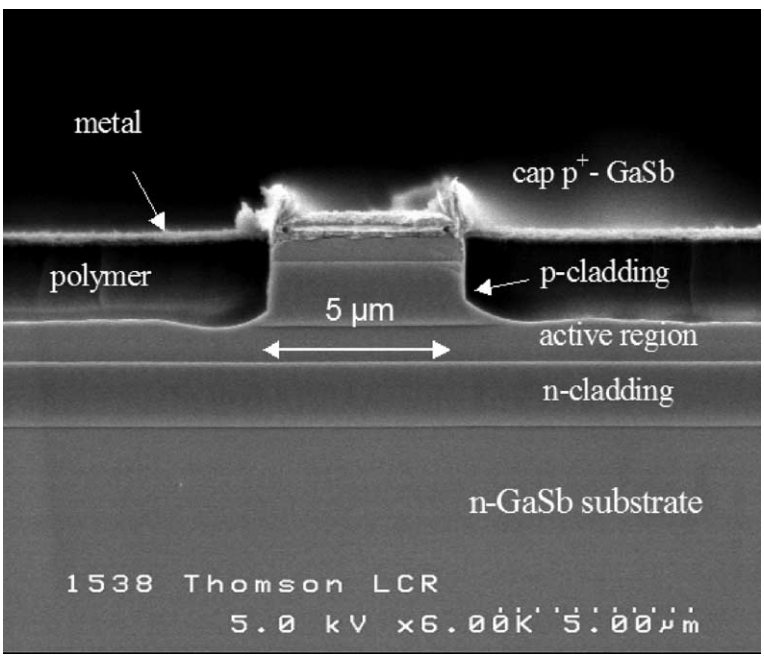

Fig. 10. Cross section of a ridge type-I GaInAsSb/AlGaAsSb QW laser diode.

Such type-I GaInAsSb/AlGaAsSb lasers having the band structure of Fig. 9 emitted CW at room temperature near 2.3 µm with low threshold current, varying from 100 to 300 $\mathrm{A/cm^2}$ depending on the cavity length and the number of quantum wells. The characteristic temperature T_0, which indicates the temperature sensitivity of the threshold current $I_{\mathrm{th}} = I_0 \exp(T/T_0)$, is higher than 100 K. The external differential quantum efficiency α_{d}, defined as the ratio of the number of emitted photons per second on the number of injected electrons per second is ∼40–60%. Linear relationships between $1/\eta_{\mathrm{d}}$ and the cavity length were observed, furnishing typical internal loss coefficient $\alpha_{\mathrm{int}} \sim 10\ \mathrm{cm^{-1}}$ and internal quantum efficiency $\eta_{\mathrm{int}} \sim 60$–80%.

For broad area lasers, the emission spectrum shows longitudinal and transverse modes. The CW output power is high with a maximum value close to 1 W. The plug power efficiency is ∼10%. In pulsed-current mode the peak power is nearly 5 W. These results are excellent, and could be still improved by reducing the thermal resistance of the mounted device, as predicted in Fig. 11.

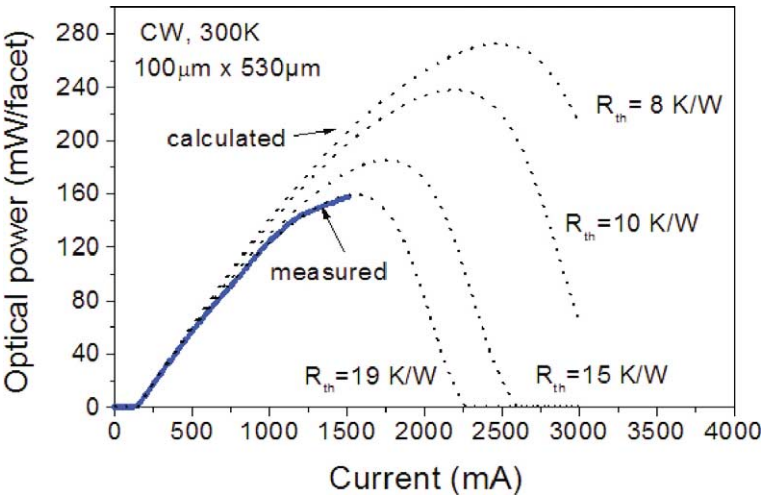

Fig. 11. Influence of the thermal resistance of the mounted diode on the output power – current characteristic, after Perona [94].

For narrow ridge lasers, transverse modes are suppressed and, in some cases, only one longitudinal mode is observed. Lasing wavelength can be changed by varying the injection current or the temperature. The tuning rate versus current is ∼0.02 nm/mA, and the temperature tuning is of the order of 1 nm/°C. The current threshold is small (20–60 mA), with a characteristic temperature of 110–130 K, and an emitted power higher than 10 mW in CW regime. This kind of lasers could emit CW above RT up to 140 °C, and up to 180 °C in pulsed regime [21] providing a very large temperature tuning interval by simple heating. Industrial applications need data about the lifetime of the devices. A lifetime of more than 15 000 hours of CW operation has been demonstrated [61] with such a type-I GaInAsSb/AlGaAsSb laser diode emitting around 2.27 μm.

By increasing the indium and arsenic content of the GaInAsSb solid solution emission wavelength can be increased from 2.0 to 2.78 μm [15,18]. A weak degradation of the threshold current density (per QW) and maximum CW output power performance is noted up to $\lambda = 2.6$ μm, which can be attributed to two factors: the reduction of valence band-offset ΔE_v inducing a loss in hole confinement, and the increasing importance of the Auger process with wavelength. Beyond 2.6 μm, a brutal deterioration is observed, certainly due to the fact that compositions of the GaInAsSb QWs having effective band gap energies higher than 2.7 μm lie inside the solid phase miscibility gap of the quaternary alloy [62].

4. Type-II GaInAsSb/GaSb laser diodes

In relation to the type-I GaInAsSb/AlGaAsSb QW system, type-II GaInAsSb/GaSb system offers two main important advantages: (i) a smaller Auger rate ($C_{\text{Auger}} \sim 5 \times 10^{-29}$ cm^6/s at 2.35 μm); and (ii) the possibility to extend the emission wavelength beyond 2.8 μm, up to 3.5 μm [40]. The problem for type-II heterostructures is the weak overlap of electron and hole wavefunctions, electrons being localized in one layer (quantum well) while holes are localized in another (GaSb barrier). The consequence is a weak optical efficiency and a strong increase in current threshold. In fact, it was demonstrated [40] that under injection, the localised electrons in the quantum well 'pull' the holes from the adjacent GaSb barrier due to Coulomb interaction. Such an interaction induces a modification of the band structure near the heterointerfaces, generating narrow quantum wells in the GaSb barriers (Fig. 12). Consequently, holes are confined in a nearly triangular potential close to the QW interfaces, and their presence probability near the quantum well is strongly increased so that the electron–hole wavefunction overlap becomes important. In these conditions, the reported good performance from type-II GaInAsSb/GaSb QW lasers are not surprising [19, 22,63–67].

The initial structure [64] contained five 7-nm-thick $Ga_{0.65}In_{0.35}Sb_{0.85}As_{0.15}$ quantum wells between 30-nm-thick GaSb barriers, the total thickness of the active zone being 0.3 μm. The wells and the barriers had a type-II band alignment with a valence band offset ΔE_v of 80 meV (the heavy hole subband for the QW) and a conduction band offset $\Delta E_c = 350$ meV. The wide mesa lasers emitted between 2.35 μm and 2.39 μm at room temperature. The threshold current density monotically decreases from 2.5 kA/cm^2 to 400 A/cm^2 when the cavity length increases from 200 μm to 1500 μm. The characteristic temperature was $T_0 = 60$ K. Ridge waveguide 8-μm-wide lasers operating in CW regime at RT were fabricated from a similar wafer [67]. The lasers had threshold currents in the range 60–140 mA and emitted 2 to 5 mW/facet of optical power in the range of 2.34–2.4 μm.

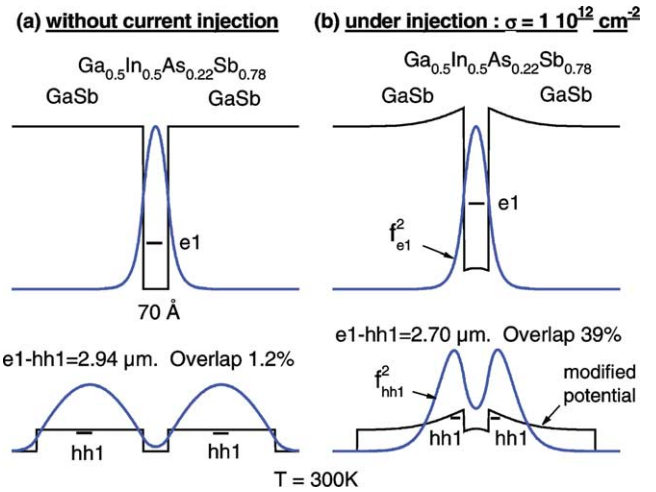

Fig. 12. Energy band diagram of $Ga_{0.5}In_{0.5}As_{0.22}Sb_{0.78}$/GaSb quantum well and carrier probability density of presence: (a) at equilibrium; and (b) under carrier injection $\sigma_e = 1 \times 10^{12}$ cm^{-2}. The carrier wavelength overlap is increased from 1.2% to 39%, after Christol et al. [40].

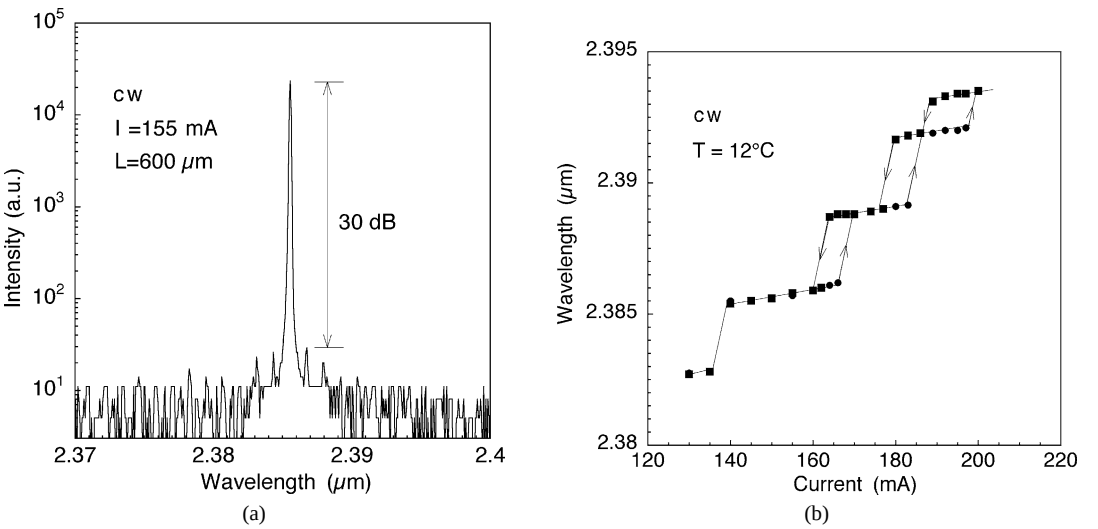

Fig. 13. (a) Emission spectrum of a type-II GaInAsSb/GaSb laser diode measured at 10 °C; and (b) dependence of the peak wavelength on current, after Yarekha et al. [22].

The emission wavelength of the type-II lasers with GaSb barriers was increased to 2.65 µm by use of the $Ga_{0.5}In_{0.5}Sb_{0.78}$–$As_{0.22}$ alloy in the 7-nm-thick wells [66]. A pulsed threshold current density of 1.5 kA/cm^2 with a characteristic temperature $T_0 = 45$ K has been obtained for 80-µm-wide devices. Total peak output power reached 130 mW with a differential quantum efficiency of 14%. From the cavity length dependence of the reciprocal external differential quantum efficiency for 2.35 µm $Ga_{0.65}In_{0.35}Sb_{0.85}As_{0.15}$/GaSb and 2.65 µm $Ga_{0.5}In_{0.5}Sb_{0.78}As_{0.22}$/GaSb type-II laser structures, the internal quantum efficiency η_{int} and the internal loss α_{int} were found to be 45% and 17 cm^{-1} for 2.35 µm laser and 33% and 62 cm^{-1} for 2.65 µm laser. The relatively high values of internal efficiency, for both type-II QW structures, were explained by the Coulomb enhancement under injection [40].

Employing broadened 0.8-µm-thick waveguide and an optimized QW growth procedure internal losses were reduced from 17 to 7.8 cm^{-1} and the laser performances were considerably improved [22]. The 10 µm ridge lasers operated in CW regime up to 50 °C with an output power of 20 mW/facet at RT. The internal quantum efficiency was found to be 89% and the power efficiency reached 20%. The lasers exhibited single frequency operation in a large range of currents and temperatures. The side mode suppression ratio reached 30 dB (Fig. 13(a)) and was nearly constant between longitudinal mode hops. Hysteresis was observed in the lasing wavelength versus current characteristics (Fig. 13(b)), which indicated autostabilization of the main

mode. The high side mode suppression ratio (SMSR), comparable with that of DFB lasers, and the observed autostabilization of the lasing mode have been explained by the photorefractive effect due to DX centers in the Te-doped $Ga_{0.4}Al_{0.6}Sb_{0.95}As_{0.05}$ cladding layer acting as a periodic saturable absorber.

Like type-I GaInAsSb/AlGaAsSb laser diodes, Fabry–Pérot devices based on type-II GaInAsSb/GaSb system appear really interesting for gas analysis by TDLAS. Their performance in the 2.0–2.6 μm wavelength range are inferior to those of type-I lasers, partly because the optical efficiency – despite Coulomb interaction positive effect – is smaller, partly because near 2 μm the electron confinement in quantum wells with GaSb barriers is lower than that due to AlGaAsSb barriers. However, around 2.7 μm and beyond, type-II GaInAsSb/GaSb QW lasers could constitute a way for achieving CW RT laser emission, specially in the 2.7–3.5 μm wavelength range.

5. Type-III InAs/GaInSb 'W' laser diodes

To achieve laser emission in the 3–5 μm mid-wavelength infrared region, a wide variety of Sb-based systems, grown on GaSb or InAs substrates, have been investigated. There are InAsSb/InAsPSb [68,69] and GaInAsSb/AlGaAsSb [70] double-heterostructure lasers, type-I or type-II quantum well lasers with InAsSb/InAs [71–73], InAsSb/InAlAsSb [47, 74], InAsSb/InAsP [75,76] or InSb/AlInSb [77] heterostructures. All these traditional systems have presented excellent performances at low temperatures, but laser emission was limited to 225 K in pulsed regime and to 175 K in CW regime (Fig. 4) [47].

To improve the maximum temperature of operation T_{max}, a new laser design has been proposed based on interband type-II broken gap InAs/GaInSb/InAs 'W' structures [23]. The designed active region is made of several QW periods, each period including a GaInSb 'hole' quantum well sandwiched between a double InAs 'electron' quantum wells, what forms a conduction band profile in the shape of a 'W' (Fig. 14). This system presents several advantages. First, the 'W' arrangement induces a phase position of the carriers that increases the electron–hole overlap integral and hence the optical matrix elements, giving values comparable to type-I structures. Next, this structure keeps the advantages of type-II ones like a substantial reduction of Auger recombination [54,57] and internal losses [78], because of the small in-plane electron and hole masses and the elimination of the resonance between the energy gap and the split-off valence band or with any other lower valence sub-bands.

Excellent results have been obtained by the 'W' structure design reported in Fig. 14 [24–26]. The active region consisted of five or ten W periods of InAs (15 Å)/$Ga_{0.75}In_{0.25}Sb$ (27 Å)/InAs (15 Å) separated by AlGaAsSb (80 Å) spacer layer. This layer furnishes a two-dimensional dispersion for both electrons and holes with strong confinement in each 'W' period. These MQWs are embedded in a 0.6 μm thick AlGaAsSb waveguide layer to maximise the optical confinement factor Γ in the active region, while minimizing free-carrier absorption losses in the cladding layers. The optical cladding layers are made from AlGaAsSb, lattice-matched to GaSb. The fundamental e_1-hh_1 optical transition was expected around 3.3 μm at RT.

For a reasonable injected carrier concentration N3D $= 1 \times 10^{18}$ cm^{-3}, the calculated modal gain can reach 230 cm^{-1} at $T = 100$ K and 35 cm^{-1} at $T = 300$ K. This last value confirms that the 'W' structure can theoretically operate at RT, but

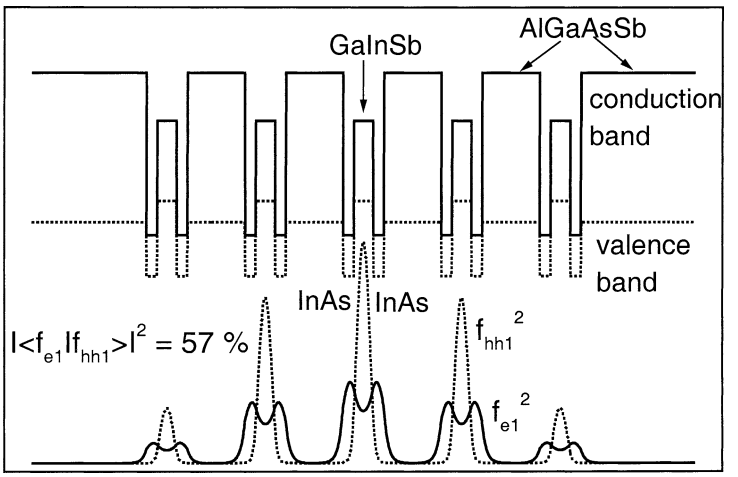

Fig. 14. Schematic band diagram of the InAs (15 Å)/GaInSb (27 Å)/InAs (15 Å)/AlGaAsSb (80 Å) 'W' laser structure. In the lower part, the fundamental electron (e_1) and heavy-hole (hh_1) presence probability densities f_{e1}^2 and f_{hh1}^2 are reported. The carrier wavefunction overlap is 57%.

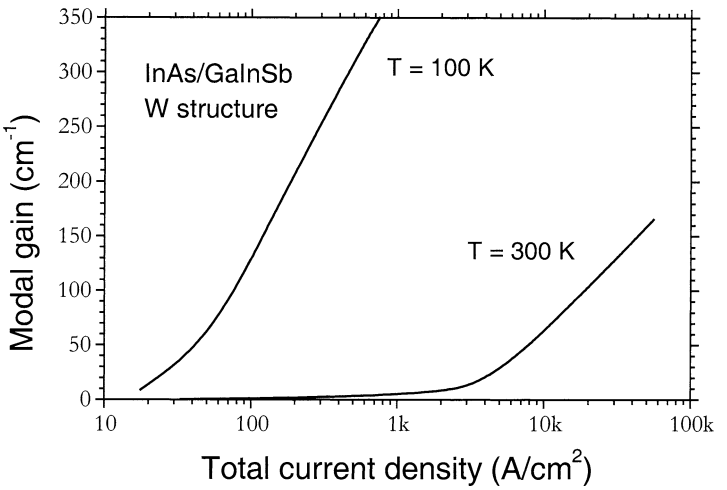

Fig. 15. Modal gain G_{mod} versus total current density J (A/cm^2) calculated at $T = 100$ K and $T = 300$ K. The active region is composed of ten 'W' periods.

only for laser structures having small optical losses with excellent structural quality of the grown layers. Modal gain versus total current density J (Eq. (2)) is shown in Fig. 15. Standard values for Sb-based structures are considered [79]: the non-radiative recombination coefficient $A = 108\ \mathrm{s}^{-1}$ can be taken as temperature independent; the radiative coefficient B was taken equal to 7×10^{-11} cm^3/s and 4×10^{-11} cm^3/s and the Auger coefficient C, which governs the current, was fixed at $C = 5 \times 10^{-29}$ cm^6/s and $C = 5 \times 10^{-27}$ cm^6/s, at $T = 100$ K and $T = 300$ K, respectively. The theoretical results confirm the experimental values reported in [24,25] with a threshold current density of 16 kA/cm^2 at 300 K.

The laser devices were processed into 100 μm-wide stripes. In pulsed regime (0.2–0.5 μs, 200 Hz), the device, with ten 'W' periods, operated up to 310 K. At this temperature, the laser emission was observed at 3.27 μm, the output power was 370 μW and the threshold current density J_{th} was 25 kA/cm^2. On the other hand, in the continuous regime, the best results were obtained with five 'W' periods. At 80 K the measured threshold current density was 63 A/cm^2, and the CW output power was 140 mW. The CW lasing performances improve when the number of QWs is kept small to limit the threshold while in pulsed regime at higher temperature, the ten-period devices outperformed the five ones because important gain is needed. CW measurements yielded a maximum operating temperature of 195K with a threshold current density of 1.4 kA/cm^2 and a characteristic temperature $T_0 = 38$ K [25]. To date, this result is the highest CW operation temperature T_{max} for the III-V mid-infrared laser diodes.

6. Type-III interband InAs/GaSb/AlSb quantum cascade lasers (ICLs)

In the QC laser the conduction band discontinuity between the two semiconductor materials would be much higher than inter sub-band transition energy in order to avoid electron leakage above the quantum well. This is not the case in the 3–5 μm range with type-I QC lasers based on InP lattice-matched $Ga_{0.47}In_{0.53}As/Al_{0.48}In_{0.52}As$ system ($\Delta E_c = 520$ meV). A means to increase the band discontinuity is to employ strain compensated GaInAs/AlInAs layers ($\Delta E_c = 740$ meV for $Ga_{0.3}In_{0.7}As/Al_{0.6}In_{0.4}As$ system). QC lasers based on these materials could emit at shorter wavelengths up to 3.4 μm [29].

Another system was proposed for the realisation of inter sub-band QC lasers operating in the 3–5 μm wavelength range: the InAs/AlSb system grown on GaSb substrate [80]. The very high conduction band discontinuity (2.1 eV at Γ points) of this material system allows the design of QC devices at short wavelengths. First results are encouraging, and efforts are being made to improve the design of the QC structure to achieve laser emission at room temperature [81].

In these type-I quantum-well lasers the main problem to solve is the fast non-radiative relaxation between sub-bands via optical phonon scattering, of the order of 1 ps, leading to a low radiative efficiency and to a substantial heating which limit their performances. By using a new class of quantum cascade lasers based on resonant interband tunnelling in a leaky type-III broken-gap system, it is still possible to improve the characteristics of these QC lasers [34,82,83]. The type-III broken-gap alignment provides two necessary conditions for achieving an efficient population inversion: a good confinement of electrons at the upper energy and, due to the existence of a window near the bottom of the well, a fast electron tunnelling rate at the lower level. The most appropriate system for the design of such structures is the type-III InAs/Ga(In)Sb/AlSb poly-type material system where the radiative transitions arise from InAs/GaSb or InAs/GaInSb quantum wells.

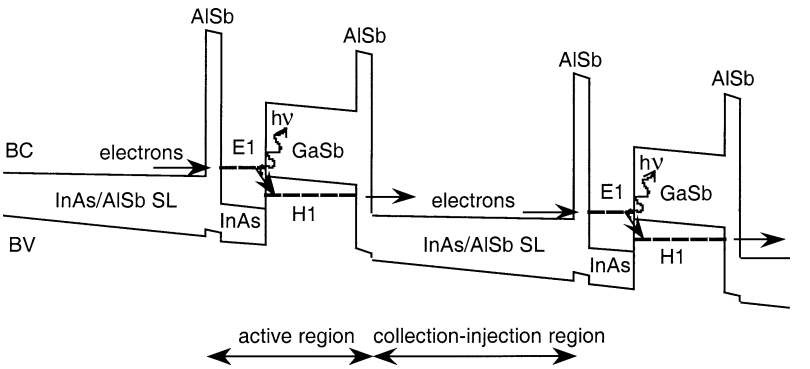

Fig. 16. Band diagram (not to scale) under bias of a quantum cascade laser based on interband transitions in a AlSb/InAs/GaSb quantum well structure, following references [34,82,84].

A type-III interband QC laser using the InAs/AlSb/GaSb system is shown in Fig. 16 [34,82,84]. The basic unit of this structure comprises two coupled InAs/GaSb QWS, which are designed to have, under an external electric field applied along the growth direction, the ground electron level E_1 in the InAs QW above the valence band edge of GaSb, and the ground hole level H_1 in the GaSb QW above the conduction band edge of InAs. Electrons enter from the left and are injected by resonant tunnelling from the injection region (a graded AlInAsSb solid solution or a digitally graded InAs/AlSb superlattice) into the InAs quantum well. They are blocked by GaSb and AlSb barriers which prevent tunnelling to the next collection/injection region and may escape only by making optical transitions to the valence band of the GaSb quantum well. They finally transfer to the collection region through elastic interband tunnelling.

The main advantage of this type-III interband QC laser towards an intersubband QC laser is the suppression of the non-radiative relaxation between the two states via optical phonons. Another advantage is the substantial penetration of the light-hole state into the InAs QW, while the heavy-hole state is localized inside the GaSb QW [82]. Thus a strong spatial interband coupling is provided between electrons and light holes whereas the spatial interband coupling between the electrons and heavy holes is very weak. This feature has two positive effects. First the CHCC and the CHHH Auger recombination processes involving an electron-heavy hole recombination are small. Next the population inversion between the two transition states is easily achieved due to the high interband tunnelling rate of the light holes ($\sim$0.1 ps). As a consequence the radiative efficiency can be very high in this type-III interband QC laser.

IC lasers were first demonstrated in early 1997 [85]. Shortly thereafter, type-III IC lasers were improved, with encouraging results: $\sim$0.5 W/facet peak power, relatively high external differential quantum efficiency ($>$200%), high temperature operation at 3.5 μm [86–88]. In 1999, significant advances [35,36,89] were made in the development of IC lasers. The laser structure, grown on a p-type GaSb substrate, had about 20 repeated periods of active regions separated by n-type injection regions, that form the waveguide core. Two n-type InAs/AlSb superlattices were used as top and bottom optical waveguide cladding layers, with thicknesses of $\sim$2 μm. Digitally graded InAs/AlInSb multiquantum wells were employed for the injection region, which serves as a collector for the preceding active region and as an emitter for the following one. Each active region comprised coupled QWs, stacked sequentially with as an example [89] 23 Å AlSb, 25 Å InAs, 36 Å $Ga_{0.7}In_{0.3}Sb$, 15 Å AlSb, and 58 Å GaSb layers. Electrons injected into the first InAs quantum well emit a photon by making a type-III interband optical transition to the valence band of the GaInSb hole quantum well. They next tunnel across the AlSb barrier into the valence band of the adjacent GaSb hole well, from which they can make the transfer mentioned above to the conduction band of the first InAs quantum well of the injected region. Excellent results have been reported from ICLs having this design: record external differential quantum efficiency ($\sim$500%) and high peak output power ($>$4 W/facet) at 80 K, increased maximum temperature of operation (217 K) at emission wavelengths 3.8–3.9 μm, and peak power efficiency of $\sim$7%.

IC lasers with a similar structure but designed for 3.6–3.8 μm emission, could emit in the continuous wave mode up to 127 K (250 K pulsed) [48]. Fig. 17 shows the current-voltage-light characteristics for such a laser under CW conditions. The operating voltage is $\sim$6.5 V, only $\sim$107% of the minimum voltage required in an ideal case (number of periods multiplied by the photon energy in eV). It presents no obvious change in the temperature range from 60 to 120 K. An abrupt reduction of the differential resistance was observed at the threshold, as shown in the bottom of Fig. 17. At 80 K the threshold current density is as low as 56 A/cm^2, the CW optical power is 25 mW/facet (at a current level $I = 100$ mA) and the differential power efficiency is 391 mW/A, corresponding to a differential external quantum efficiency of 232%. The power efficiency at 80 K is 7.5% (at 100 mA).

A noticeable improvement is expected at high temperature using type-III active region with the 'W' geometry. As discussed in Section 5 the enhancement of the carrier wavefunction overlap would increase the differential gain and, consequently, lower

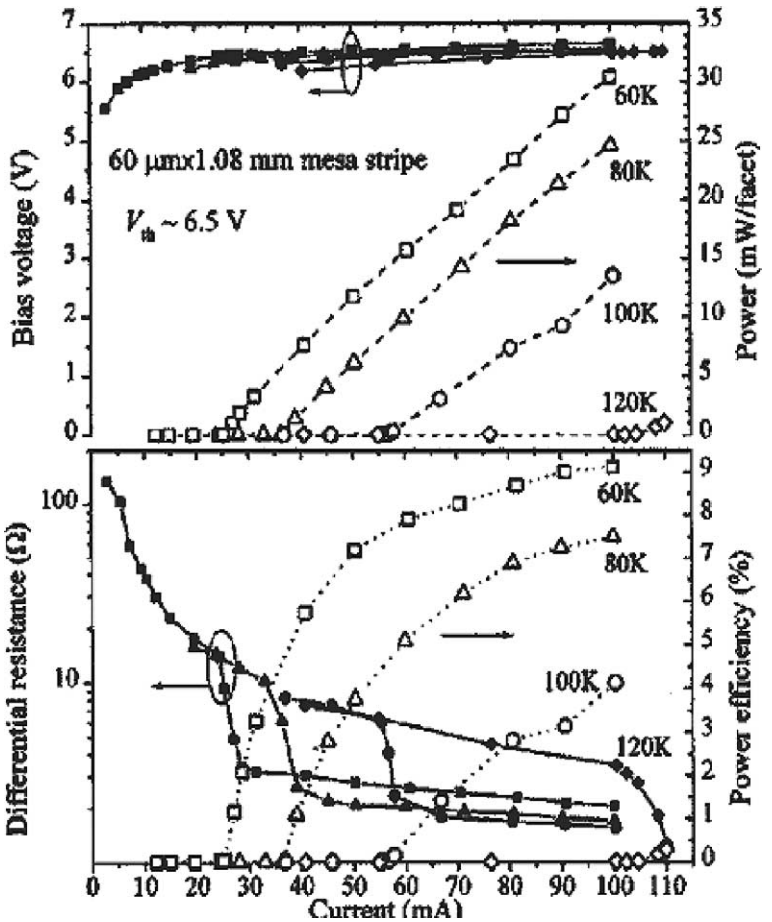

Fig. 17. CW operation of a mesa-stripe InAs/GaInSb IC laser at several temperatures. Voltage-current and output power-current characteristics (top), differential resistance and power efficiency versus current (bottom), after Bruno et al. [48]. Published with permission of the authors, and the American Institute of Physics.

the threshold current density. IC lasers with W active region were grown on p-type GaSb substrates with similar structures to the above ICLs, but including additional InAs QW inserted between the GaInSb and AlSb layers in each active region [90–93]. No improvement was observed concerning output power efficiency, but higher temperature of pulsed operation could be achieved (up to 300 K [93]) for such 'W'-ICLs emitting around 3.5 μm.

These type-III IC lasers offer numerous variations of cascade structures, and parameters such as carrier transport, non-radiative processes, internal absorption losses, which substantially affect the laser performance, could be improved. As a consequence, interband QC lasers are still far from optimum, and well promising for the achievement of MIR injection laser devices.

7. Conclusion

Several technologies are in competition for the achievement of mid-infrared laser diodes operating CW at room temperature: type-I GaInAsSb/AlGaAsSb MQW lasers, type-II GaInAsSb/GaSb MQW lasers, lead salt lasers, inter sub-band GaInAs/InAlAs and InAs/AlSb quantum cascade lasers, type-III 'W' InAs/GaInSb lasers, and interband cascade lasers based on the same system.

In the 2.0–2.6 μm wavelength range impressive results have been obtained from type-I quantum well GaInAsSb-AlGaAsSb lasers: CW output powers of the order of 1 W/facet at 300 K, threshold current densities of 50–150 A/cm^2, characteristic temperatures T_0 higher than 100 K, CW operation up to 140 °C, high internal efficiencies and extremely small internal loss coefficient (as low as ~2 cm^{-1}). Gas detection by TDLAS using Fabry–Pérot ridge laser diodes operating around 2.3 μm was

successfully demonstrated. In that range of wavelengths, type-I GaInAsSb/AlGaAsSb MQW laser diodes appear as the best and already well-established technology.

Beyond 2.6 μm the other technologies under consideration showed encouraging performance, but they must be optimised to achieve the goal of CW mid-infrared emission at room temperature.

References

[1] H.A. Gebbie, W.R. Harding, C. Hilsum, A.W. Pryce, V. Roberts, Atmospheric transmission in the 1 to 14 μm region, Proc. Roy. Soc. A 206 (1951) 87.

[2] L.S. Rothman, R.R. Gamache, H.H. Tipping, C.P. Rinsland, M.A.H. Smith, D.C. Benner, V.M. Devi, J.M. Flaud, C. Camy-Peyret, A. Perrin, A. Goldman, S.T. Massie, L.R. Brown, R.A. Toth, The HITRAN molecular data base: editions of 1991 and 1992, J. Quantum Spectrosc. Radiat. Transf. 48 (1992) 469.

[3] H.I. Schiff, G.I. Mackay, J. Bechara, The use of tunable diode laser absorption spectroscopy for atmospheric measurements, in: M.W. Sigrist (Ed.), Air Monitoring by Spectroscopy Techniques, Wiley, New York, 1994.

[4] I. Melngailis, Maser action in InAs diodes, Appl. Phys. Lett. 2 (1963) 176–178.

[5] J. Phelan, A.R. Calawa, R.H. Rediker, R.J. Keyes, B. Lax, Infrared InSb laser diodes in high magnetic fields, Appl. Phys. Lett. 3 (1963) 143–145.

[6] C.B. Guillaume, P. Lavallard, Laser effect in indium antimonide, Solid State Comm. 1 (1963) 148–150.

[7] Y. Horikoshi, Semiconductor lasers with wavelengths >2 μm, in: W.T. Tsang (Ed.), Semiconductors and Semimetals 22, Academic Press, London, 1985, pp. 93–151, Chapter 3.

[8] D.L. Partin, C.M. Trush, Wavelength coverage of lead-europium-selenide-telluride diode lasers, Appl. Phys. Lett. 45 (1984) 193–195.

[9] G. Bauer, M. Kriechbaum, Z. Shi, M. Tacke, IV-VI quantum wells for infrared lasers, J. Nonlinear Opt. Phys. Mater. 4 (1995) 283–312.

[10] Z. Shi, M. Tacke, A. Lambrecht, H. Böttner, Midinfrared lead salt multi-quantum-well diode lasers with 282 K operation, Appl. Phys. Lett. 66 (1995) 2537–2539.

[11] M. Tacke, Lead salt lasers, Philos. Trans. Roy. Soc. London Ser. A 359 (2001) 547–566.

[12] H. Preir, Physics and applications of IV-VI compound semiconductor lasers, Semicond. Sci. Technol. 5 (1990) S12–S20.

[13] E.P. O'Reilly, A.R. Adams, Band structure engineering in strained semiconductor lasers, IEEE J. Quantum Electron. 30 (1994) 366–379.

[14] C.R. Ram-Mohan, J.R. Meyer, Multiband finite element modelling of wavefunction engineered electro-optical devices, J. Nonlinear Opt. Phys. Mat. 4 (1995) 191–243.

[15] D.Z. Garbuzov, H. Lee, V. Khalfin, R. Martinelli, J.C. Connolly, G.L. Belenky, 2.3–2.7 μm room temperature CW operation of InGaAsSb-AlGaAsSb broad waveguide SCH-QW diode lasers, IEEE Photon. Technol. Lett. 11 (1999) 794–796.

[16] H.K. Choi, S.J. Eglash, High power multiple quantum well GaInAsSb/AlGaAsSb diode lasers emitting at 2.1 μm with low threshold current density, Appl. Phys. Lett. 61 (1992) 1154–1156.

[17] H.K. Choi, G.W. Turner, S.J. Eglash, High-power GaInAsSb-AlGaAsSb multiple quantum well diode lasers emitting at 1.9 μm, IEEE Photon. Technol. Lett. 6 (1994) 7–9.

[18] H. Lee, P.K. York, R.J. Menna, R.U. Martinelli, D.Z. Garbuzov, S.Y. Narayan, J.C. Connolly, Room temperature 2.78 μm AlGaAsSb/InGaAsSb quantum well lasers, Appl. Phys. Lett. 66 (1995) 1942–1944.

[19] A.N. Baranov, N. Bertru, Y. Cuminal, G. Boissier, Y. Rouillard, J.C. Nicolas, P. Grech, A. Joullié, C. Alibert, Mid-infrared GaSb-InAs based multiple quantum well lasers, SPIE 3284 (1998) 247–255.

[20] A. Joullié, New developments in mid-infrared Sb-based lasers, J. Phys. IV (France) 9 (1999) Pr2.79–Pr2.96.

[21] D.A. Yarekha, G. Glastre, A. Perona, Y. Rouillard, F. Genty, E.M. Skouri, G. Boissier, P. Grech, A. Joullié, C. Alibert, A.N. Baranov, High temperature GaInAsSb/GaAlAsSb quantum well singlemode continuous wave lasers emitting near 2.3 μm, Electron. Lett. 36 (2000) 537–539.

[22] D.A. Yarekha, A. Vicet, A. Perona, G. Glastre, B. Fraisse, Y. Rouillard, E.M. Skouri, G. Boissier, P. Grech, A. Joullié, C. Alibert, A.N. Baranov, High efficiency GaInAsSb/GaSb type-II quantum well continuous wave lasers, Semicond. Sci. Technol. 15 (2000) 283–288.

[23] J.R. Meyer, C.A. Hoffman, F.J. Bartoli, L.R. Ram-Mohan, Type-II quantum well lasers for the mid-wavelength infrared, Appl. Phys. Lett. 67 (1995) 757–759.

[24] H. Lee, L.J. Olafsen, R.J. Menna, W.W. Bewley, R.U. Martinelli, I. Vurgaftman, D.Z. Garbuzov, C.L. Felix, M. Maiorov, J.R. Meyer, J.C. Connolly, A.R. Stugg, G.H. Olsen, Room-temperature type-II quantum well diode laser with broadened waveguide emitting at $\lambda = 3.30$ μm, Electron. Lett. 35 (1999) 1743–1745.

[25] W.W. Bewley, H. Lee, I. Vurgaftman, R.J. Menna, C.L. Felix, R.U. Martinelli, D.W. Stokes, D.Z. Garbuzov, J.R. Meyer, M. Maiorov, J.C. Connolly, A.R. Stugg, G.H. Olsen, Continuous-wave operation of $\lambda = 3.25$ μm broadened-waveguide W quantum-well diode lasers up to $T = 195$ K, Appl. Phys. Lett. 6 (2000) 256–258.

[26] B.I. Vurgaftman, C.L. Felix, W.W. Bewley, D.W. Stokes, R.E. Bartolo, J.R. Meyer, Mid-infrared 'W' lasers, Philos. Trans. Roy. Soc. London Ser. A 359 (2001) 489–503.

[27] J. Faist, F. Capasso, D.L. Sivco, C. Sirtori, A.L. Hutchinson, A.Y. Cho, Quantum cascade laser, Science 264 (1994) 553–556.

[28] R. Köhler, C. Gmachl, A. Tredicucci, F. Capasso, D.L. Sivco, S.N. George Chu, A.Y. Cho, Single-mode tunable, pulsed, and continuous wave quantum-cascade distributed feedback lasers at $\lambda = 4.6$–4.7 μm, Appl. Phys. Lett. 76 (2000) 1092–1094.

[29] J. Faist, F. Capasso, D.L. Sivco, A.L. Hutchinson, G. Chu Sung-Nee, A.Y. Cho, Short wavelength ($\lambda \sim 3.4$ μm) quantum cascade laser based on strain-compensated InGaAs/AlInAs, Appl. Phys. Lett. 72 (1998) 680–682.

[30] F. Capasso, C. Gmachl, R. Paiella, A. Tredicucci, A.L. Hutchinson, D.L. Sivco, J.N. Baillargeon, A.Y. Cho, H.C. Liu, New frontiers in quantum cascade lasers and applications, IEEE J. Select. Topics Quantum Electron. 6 (2000) 931–947.
[31] F.Q. Liu, Y.Z. Zhang, Q.S. Zhang, D. Ding, X. Bo, Z.G. Wang, D.S. Jiang, B.Q. Sun, High-performance strain-compensated InGaAs/InAlAs quantum cascade lasers, Semicond. Sci. Technol. 15 (2000) L44–L46.
[32] F. Capasso, Optics & Photonics News, May 2001, p. 41.
[33] B. Ishaug, W.Y. Hwang, J. Um, B. Guo, H. Lee, C.H. Lin, Continuous-wave operation of a 5.2 μm quantum-cascade laser up to 210 K, Appl. Phys. Lett. 79 (2001) 1747–1749.
[34] R.Q. Yang, Infrared lasers based on intersubband transitions in quantum wells, Superlatt. Microstr. 17 (1995) 77–83.
[35] R.Q. Yang, J.D. Bruno, J.L. Bradshaw, J.T. Pham, D.E. Wortman, High-power interband cascade lasers with quantum efficiency >450%, Electron. Lett. 35 (1999) 1254–1255.
[36] R.Q. Yang, J.D. Bruno, J.L. Bradshaw, J.T. Pham, D.E. Wortman, Interband cascade lasers: progress and challenges, Physica E 7 (2000) 69–75.
[37] D.H. Chow, R.H. Miles, T.C. Hasenberg, A.R. Kost, Y.H. Zhang, H.L. Dunlap, L. West, Midwave infrared diode lasers based on GaSb/InAs and InAs/AlSb superlattices, Appl. Phys. Lett. 67 (1995) 3700–3702.
[38] D.Z. Garbuzov, R.U. Martinelli, H. Lee, P.K. York, R.J. Menna, J.C. Connolly, S.Y. Narayan, Ultra low-loss broadened-waveguide high-power 2 μm AlGaAsSb/InGaAsSb/GaSb separate-confinement quantum-well lasers, Appl. Phys. Lett. 69 (1996) 2006–2008.
[39] M.P. Krijn, Heterojunction band offsets and effective masses in III-V quaternary alloys, Semicond. Sci. Technol. 6 (1991) 27–31.
[40] P. Christol, P. Bigenwald, A. Joullié, Y. Cuminal, A.N. Baranov, N. Bertru, Y. Rouillard, Improvement of Sb-based multiquantum well lasers by Coulomb enhancement, IEE Proc.-Optoelectron. 146 (1999) 3–8.
[41] Y. Tsou, A. Ichii, E.M. Garmire, Improving InAs double heterostructure lasers with better confinement, IEEE J. Quantum Electron. 28 (1992) 1261–1268.
[42] Z. Feit, M. Mc Donald, R.J. Woods, V. Archambault, P. Mak, Low threshold PbEuSeTe/PbTe separate confinement buried heterostructure diode lasers, Appl. Phys. Lett. 68 (1996) 738–740.
[43] D. Garbuzov, R.U. Martinelli, H. Lee, R.J. Menna, P.K. York, L.A. DiMarko, M.G. Harvey, R.J. Matarese, S.Y. Narayan, J.C. Connolly, 4W quasi-continuous-wave output power from 2 μm AlGaAsSb/InGaAsSb single-quantum-well broadened waveguide laser diodes, Appl. Phys. Lett. 70 (1997) 2931–2933.
[44] R.J. Menna, D.Z. Garbuzov, H. Lee, R.U. Martinelli, S.J. Narayan, J.C. Connolly, High power broadened-waveguide InGaAsSb/AlGaAsSb quantum-well diode lasers emitting at 2 μm, SPIE Proc. 3284 (1998) 238–246.
[45] M. Garcia, A. Sahli, C. Becker, A. Pérona, Y. Rouillard, C. Sirtori, X. Marcadet, Low threshold high power efficiency room temperature continuous wave operation diode laser emitting at 2.26 μm, submitted.
[46] J.G. Kim, L. Shterengas, R.U. Martinelli, G.L. Belenky, D.Z. Garbuzov, W.K. Chan, Room temperature 2.5 μm InGaAsSb/AlGaAsSb diode lasers emitting 1W continuous waves, Appl. Phys. Lett. 81 (2002) 3146–3148.
[47] H.K. Choi, G.W. Turner, M.J. Manfra, High CW power (>200 mW/facet) at 3.4 μm from InAsSb/InAlAsSb strained quantum well diode lasers, Electron. Lett. 32 (1996) 1296–1297;
See also H.K. Choi, G.W. Turner, M.J. Manfra, M.K. Connors, 175 K continuous wave operation of InAsSb/InAlAsSb quantum well diode lasers emitting at 3.5 μm, Appl. Phys. Lett. 68 (1996) 2936–2938.
[48] J.D. Bruno, J.L. Bradshaw, R.Q. Yang, J.T. Pham, D.E. Wortman, Low threshold interband cascade lasers with power efficiency exceeding 9%, Appl. Phys. Lett. 76 (2000) 3167–3169.
[49] G.P. Agrawal, N.K. Dutta, in: S. Mitra (Ed.), Long Wavelength Semiconductor Lasers, Van Nostrand–Reinhold, New York, 1986.
[50] B.K. Ridley, Quantum Processes in Semiconductors, Clarendon Press, Oxford, 1988.
[51] E. Rosencher, B. Vinter, Optoélectronique, Masson, Paris, 1998, pp. 265–271.
[52] A. Haug, Auger recombination in quantum well semiconductors: calculation with realistic energy bands, Semicond. Sci. Technol. 7 (1992) 1337–1340.
[53] H.Y. Fan, in: O. Willardson, O. Beer (Eds.), Semiconductors and Semimetals, Vol. 3, Academic Press, New York, 1967, Chapter 9.
[54] C.H. Grein, P.M. Young, H. Ehrenreich, Theoretical performance of InAs/$In_xGa_{1-x}Sb$ superlattice-based midwave infrared lasers, J. Appl. Phys. 76 (1994) 1940–1942.
[55] G.G. Zegrya, A.D. Andreev, Mechanism of suppression of Auger recombination processes in type-II heterostructures, Appl. Phys. Lett. 67 (1995) 2681–2683.
[56] J.I. Malin, J.R. Meyer, C.L. Felix, Type-II mid-IR lasers operating at room temperature, Appl. Phys. Lett. 68 (1996) 2976–2978.
[57] J.R. Meyer, C.L. Felix, W.W. Bewley, et al., Auger coefficients in type-II InAs/$Ga_{1-x}In_xSb$ quantum wells, Appl. Phys. Lett. 73 (1998) 2857–2859.
[58] J.L. Pautrat, reported, in: E. Rosencher, B. Vinter (Eds.), Optoélectronique, Masson, Paris, 1998, p. 234.
[59] A. Haug, D. Kerkhoff, W. Lochmann, Calculation of Auger coefficients for III-V compounds with emphasis on GaSb, Phys. Status Solidi B 89 (1978) 357–365.
[60] A.R. Adams, Band structure engineering for low threshold high efficiency semiconductor lasers, Electron. Lett. 22 (1986) 249–250.
[61] A. Vicet, D.A. Yarekha, A. Perona, Y. Rouillard, S. Gaillard, A.N. Baranov, Trace gas detection with antimonide-based quantum-well diode lasers, Spectrochim. Acta Part A 58 (2002) 2405–2412.
[62] J.L. Lazzari, E. Tournié, F. Pitard, A. Joullié, B. Lambert, Growth limitations by the miscibility gap in the liquid phase epitaxy of $Ga_{1-x}In_xAs_ySb_{1-y}$ on GaSb, Mater. Sci. Engrg. B 9 (1991) 125–128.
[63] A.N. Baranov, Y. Cuminal, N. Bertru, C. Alibert, A. Joullié, Strained multiple quantum well lasers grown on GaSb emitting between 2 and 2.4 μm, SPIE 2997 (1997) 2–13.

[64] A.N. Baranov, Y. Cuminal, G. Boissier, C. Alibert, A. Joullié, Low-threshold laser diodes based on type-II GaInAsSb/GaSb quantum-wells operating at 2.36 μm at room temperature, Electron. Lett. 32 (1996) 2279–2280.
[65] N. Bertru, A.N. Baranov, Y. Cuminal, G. Almuneau, F. Genty, A. Joullie, O. Brandt, A. Mazuelas, K.H. Ploog, Long-wavelength (Ga, In)Sb/GaSb strained quantum well lasers grown by molecular beam epitaxy, Semicond. Sci. Technol. 13 (1998) 936–940.
[66] Y. Cuminal, A.N. Baranov, D. Bec, P. Grech, M. Garcia, G. Boissier, A. Joullié, G. Glastre, R. Blondeau, Room-temperature 2.63 μm GaInAsSb/GaSb strained quantum-well laser diodes, Semicond. Sci. Technol. 14 (1999) 283–288.
[67] A. Joullié, G. Glastre, R. Blondeau, J.C. Nicolas, Y. Cuminal, A.N. Baranov, A. Wilk, M. Garcia, P. Grech, C. Alibert, Continuous-wave operation of GaInAsSb-GaSb type-II quantum-well ridge lasers, IEEE J. Select. Topics Quantum Electron. 5 (1999) 711–715.
[68] D. Wu, B. Lane, H. Mohseni, J. Diaz, M. Razeghi, High power asymmetrical InAsSb/InAsSbP/AlAsSb double heterostructure lasers emitting at 3.4 μm, Appl. Phys. Lett. 74 (1999) 1194–1196.
[69] A. Popov, V. Sherstnev, Y. Yakovlev, R. Mücke, P. Werle, High power InAsSb/InAsSbP double heterostructure laser for continuous wave operation at 3.6 μm, Appl. Phys. Lett. 68 (1996) 2790–2792;
See also: SPIE 3001 (1997) 344–355.
[70] H.K. Choi, S.J. Eglash, G.W. Turner, Double heterostructure diode lasers emitting at 3 μm with a metastable GaInAsSb active layer and AlGaAsSb cladding layers, Appl. Phys. Lett. 64 (1994) 2474–2476.
[71] Y.H. Zhang, Continuous wave operation of InAs/InAs$_x$Sb$_{1-x}$ mid-infrared lasers, Appl. Phys. Lett. 66 (1995) 118–120.
[72] S.R. Kurtz, R.M. Biefeld, A.A. Allerman, A.J. Howard, M.H. Crawford, Pseudomorphic InAsSb multiple quantum well InAsSb lasers emitting at 3.6 μm grown by metal organic chemical vapour deposition, Appl. Phys. Lett. 68 (1996) 1332–1334.
[73] B. Lane, D. Wu, A. Rybaltowski, J. Diaz, M. Razeghi, Compressively strained multiple quantum well InAsSb lasers emitting at 3.6 μm grown by metal-organic chemical vapor deposition, Appl. Phys. Lett. 70 (1997) 443–445.
[74] G.W. Turner, M.J. Manfra, H.K. Choi, M.K. Connors, MBE growth of high power InAsSb/InAlAsSb quantum-well diode lasers emitting at 3.5 μm, J. Crystal Growth 175/176 (1997) 825–832.
[75] R.M. Biefeld, S.R. Kurtz, A.A. Allerman, The metal-organic chemical vapor deposition growth and properties of InAsSb mid-infrared (3–6 μm) lasers and LED's, IEEE J. Select. Topics Quantum Electron. 3 (1997) 739–748.
[76] B. Lane, Z. Wu, A. Stein, J. Diaz, M. Razeghi, InAsSb/InAsP strained-layer superlattice injection lasers operating at 4.0 μm grown by metal-organic chemical vapor deposition, Appl. Phys. Lett. 74 (1999) 3438–3440.
[77] T. Ashley, C.T. Elliott, R. Jefferies, A.D. Johnson, G.J. Pryce, A.M. White, M. Carroll, Mid-infrared In$_{1-x}$Al$_x$Sb/InSb heterostructure diode lasers, Appl. Phys. Lett. 70 (1997) 931–933.
[78] W.W. Bewley, I. Vurgaftman, C.L. Felix, J.R. Meyer, C.H. Lin, D. Zhang, S.J. Murry, S.S. Pei, L.R. Ram-Mohan, Role of internal loss in limiting type-II mid-IR laser performance, J. Appl. Phys. 83 (1998) 2384–2391.
[79] P. Christol, M. El Gazouli, P. Bigenwald, A. Joullié, InAs/InAs(PSb) quantum-well laser structure for the midwavelength infrared region, Physica E 14 (2002) 375–384.
[80] C. Becker, I. Prevot, X. Marcadet, B. Vinter, C. Sirtori, InAs/AlSb quantum-cascade light-emitting devices in the 3–5 μm wavelength region, Appl. Phys. Lett. 76 (2001) 1029–1031.
[81] C. Becker, H. Page, M. Calligaro, V. Ortiz, M. Garcia, X. Marcadet, C. Sirtori, GaAs- and GaSb-based quantum cascade lasers: the challenge of the new materials, in: 5th Int. Conf. Mid-Infrared Optoelectronics Materials and Devices (MIOMD-5), Annapolis, MA, 8–11 September 2002.
[82] R.Q. Yang, S.S. Pei, Novel type-II quantum cascade lasers, J. Appl. Phys. 79 (1996) 8197–8203.
[83] J.R. Meyer, I. Vurgaftman, R.Q. Yang, L.R. Ram-Moham, Type-II and type-I interband cascade lasers, Electron. Lett. 32 (1996) 45–46.
[84] R.Q. Yang, C.H. Lin, P.C. Chang, S.J. Murry, D. Zhang, S.S. Pei, S.R. Kurtz, A.N. Chu, F. Ren, Mid-IR interband cascade electroluminescence in type-II quantum wells, Electron. Lett. 32 (1996) 1621–1622.
[85] C.H. Lin, R.Q. Yang, D. Zhang, S.J. Murry, S.S. Pei, A.A. Allerman, S.R. Kurtz, Type-II interband quantum cascade laser at 3.8 μm, Electron. Lett. 33 (1997) 598–599.
[86] R.Q. Yang, B.H. Yang, D. Zhang, C.H. Lin, S.J. Murry, H. Wu, S.S. Pei, High power mid-infrared interband cascade laser based on type-II quantum wells, Appl. Phys. Lett. 71 (1997) 2409–2411.
[87] B.H. Yang, D. Zhang, R.Q. Yang, C.H. Lin, S.J. Murry, S.S. Pei, Mid-infrared interband cascade lasers with quantum efficiencies >200%, Appl. Phys. Lett. 72 (1998) 2220–2222.
[88] R.Q. Yang, Mid infrared interband cascade lasers based on type-II heterostructures, Microelectron. J. 30 (1999) 1043–1056.
[89] J.L. Bradshaw, R.Q. Yang, J.D. Bruno, J.T. Pham, D.E. Wortman, High efficiency interband cascade lasers with peak power exceeding 4W/facet, Appl. Phys. Lett. 75 (1999) 2362–2364.
[90] C.L. Felix, W.W. Bewley, I. Vurgaftman, J.R. Meyer, D. Zhang, C.H. Lin, R.Q. Yang, S.S. Pei, Interband cascade laser emitting >1 photon per injected electron, IEEE Photonics Technol. Lett. 9 (1997) 1433–1435.
[91] L.J. Olafsen, E.H. Aifer, I. Vurgaftman, W.W. Bewley, C.L. Felix, J.R. Meyer, D. Zhang, C.H. Lin, S.S. Pei, Near room temperature mid infrared interband cascade laser, Appl. Phys. Lett. 72 (1998) 2370–2372.
[92] R.Q. Yang, C.H. Lin, B.H. Yang, et al., Type-II quantum cascade lasers, Proc. SPIE 3284 (1998) 308–317.
[93] R.Q. Yang, J.L. Bradshaw, J.D. Bruno, J.T. Pham, D.E. Wortman, R.L. Tober, Room temperature type-II interband cascade laser, Appl. Phys. Lett. 81 (2002) 397–399.
[94] A. Perona, Réalisation par MBE et caractérisation physique de diodes lasers à puits quantiques GaInAsSb/AlGaAsSb émettant vers 2,3 μm, Thesis, Montpellier-II University, Montpellier (F), October 2002.